



STRONG MOTION SIMULATION OF HYOGO-KEN NANBU (KOBE) EARTHQUAKE CONSIDERING BOTH THE HETEROGENEOUS RUPTURE PROCESS AND THE 3-D BASIN STRUCTURE

Hiroshi KAWASE¹, Shinichi MATSUSHIMA², Robert W GRAVES³ And Paul G SOMERVILLE⁴

SUMMARY

We estimated strong ground motions in Kobe during the Hyogo-ken Nanbu earthquake of 1995 by using a heterogeneous rupture process and a three-dimensional (3-D) basin structure. We constructed a realistic 3-D basin model to calculate the 3-D “edge effect” which must be the cause of the damage concentration in Kobe during the earthquake. The rupture process was determined in a forward modeling procedure so that the observed bedrock motions match the synthetic waveforms. Our final source model consists of four asperities each of which has its own slip velocity function. The combination of the 3-D basin structure and the four asperity model lead us to reproduce observed strong motions in Kobe. We can conclude that we must consider the effects of the basin edge for the quantitative estimate of strong motions for future earthquakes, especially for those by active faults in inland. We also would like to emphasise the importance of the slip velocity on the rupture surface, rather than the final slip amount for near-field strong motion.

INTRODUCTION

The authors attempt to evaluate strong ground motions in the Kobe area during the Hyogo-ken Nanbu earthquake of 1995. We focus on the area that consists of Kobe city and its vicinity and try to simulate strong motion records observed within the area. Our primary goal is to prove quantitatively that we can simulate observed near-field strong motions if we use a realistic 3-D basin model and a realistic complex rupture process.

During the Hyogo-ken Nanbu earthquake of January 17, 1995 that left over 6500 casualties, the damage concentrated area, the so-called “disaster belt”, was formed along the strike of the Rokko faults. It was approximately 1 km in width and 20 km in length extending from the western end of Kobe City to the southern part of Nishinomiya City about 1 km away from the basin edge. We found that it was caused by the constructive interference of the direct S-waves coming from below and the edge-induced diffracted/surface waves generated at the edge based on two-dimensional basin response analyses and observed records [Kawase 1996]. It was named “the edge effect”, which amplified approximately 1.5 times the incident velocity pulse with predominant period of 1 second. We elucidated the amplification mechanism of the edge effect in detail [Kawase et al. 1998] and confirmed that the edge effect is not influenced by the source type as long as the incident wave field consists mainly of vertically incident S-waves.

Following these fundamental studies we attempt to generate the actual disaster belt that shows strong lateral variation to form several “disaster islands” within the disaster belt. The basin structure which stands at the northern edge of the Osaka basin is primarily a two-dimensional structure oriented from west-southwest to east-northeast sectioned by the Rokko faults. The actual basin structure in Kobe is not so simple where several buried faults can be found. The difference of the damage ratio does not necessarily mean the difference of the strong motion intensity, however, influence of a basin structure in the formation of the disaster belt is so clear that strong motion intensity must reflect the three-dimensional effects of the basin structure. Using a three-

¹ Graduate School of Human Environment Studies, Kyushu Univ., Fukuoka, Japan. kawase@seis.arch.kyushu-u.ac.jp

² Ohsaki Research Institute, Inc., Tokyo, Japan. matsui@ori.shimz.co.jp

³ Woodward Clyde Federal Services, Pasadena, U.S.A. Email: robert_graves@urscorp.com

⁴ Woodward Clyde Federal Services, Pasadena, U.S.A. Email: paul_somerville@urscorp.com

dimensional (3-D) basin structure and a source model inverted from relatively long-period strong motion records [Wald 1996], we simulated theoretical seismic motions by a 3-D finite difference method [Graves 1996]. It is found that we need to correct the source process because the original source model only provides synthetics with dominant periods longer than 2 seconds [Kawase & Matsushima 1998]. Kamae and Irikura [1998] used a relatively simple source model with three asperities to simulate strong motion at the Kobe University by CEORKA (KBU) fairly well using a semi-empirical Green's function method, although other sites such as the Kobe observatory of the Japan Meteorological Agency (JMA) could not be reproduced so well. We start from their model and try to evaluate a source model that can explain strong motion records in Kobe up to 1 second period. First we explain our 3-D basin model as well as our source model. Then we discuss on synthetics at near-source sites compared to the observed data and look at the edge-induced waves in detail.

3-D BASIN MODEL AND FAULT MODEL

A rectangle in Fig. 1 shows the area in which we model the 3-D basin structure in the Kobe region. The northwest corner of the model region is (34.645°N, 134.957°E). The area includes the intensity VII areas of the JMA scale in the Kobe region shown by the shaded areas. A small circle denotes the KBU site. The bedrock depth contours of the three-dimensional ground model used here is shown in Fig. 2 and an example of cross sections across the basin edge is shown in Fig. 3. We mapped the bedrock depths from the result of reflection surveys in between the west of JMA and Ashiya City [e.g., Endo et al. 1996, Kobayashi et al. 1996]. For other areas without detailed data we assumed a smoothed structure based on the gravity anomaly survey, geophysical surveys in the Osaka Bay, and refraction surveys [e.g. Kagawa et al. 1990]. Basin edge boundaries are picked up from the topographical and geological maps. Note that this structure is based on the information published before November 1996, and results published afterwards are not reflected yet. In most cases a steep cliff-like shape is formed at the edge, but considering that the target period band here is up to 1 second we assume a relatively smoothed bedrock structure at the close vicinity of the edge.

Table 1 shows constants used for layers inside the basin. It is assumed that each layer thickness is in proportion to the bedrock depth at a site, the ratio of which is shown in Table 1. This velocity structure was based on the P-wave velocity estimate of the reflection surveys in Kobe as well as the results of P- and S-wave velocity logging conducted in a deep boring exploration [Kobayashi et al. 1996]. It is thought that a value of 400 m/sec is appropriate as an S-wave velocity of the topmost layer of the Osaka Group formation (Pliocene), but actual ground has Pleistocene and Holocene layers whose total thickness is 10 m to 20 m in downtown areas, but is reaching more than 50 m in reclaimed land areas. We assume here, as is the case in our previous studies [Satoh et al. 1993, Kawase et al. 1995], that the nonlinear amplification characteristics including liquefaction in these layers can be evaluated separately by using one-dimensional theory and so we exclude them from this study. Table 2 shows constants of the ground model used as the Rokko Granite rock and the surrounding crustal structure. This structure is based on the structure used for the source inversion [Sekiguchi et al. 1996].

We use a 3-D finite difference method with a fourth ordered staggered-grid scheme developed by Graves [1996]. The analysed region is 42 km, 18 km, and 22.8 km in length, width, and depth or in (x, y, z) with the grid interval of 0.08 km. This grid interval yields 5 grid per wavelength for the topmost layer and 6.25 grid per wavelength for the second layer in the period of 1 second. Approximately the model has 34 million grid points and the analysis space reaches 2.4 GBytes. Time step is determined to be 0.005 sec from the stability condition and we calculate the response up to 5,000 steps. As for the surrounding boundaries we attach an ordinary transmitting boundary with the energy absorbing layers to prevent energy reflection at the boundaries. The angle of x-axis (the strike direction) is taken to be N57°E which is almost parallel to the fault strike. This choice is based on the fact that in many strong motion stations maximum principal axes of observed motions are approximately in N33°W direction.

As for the source model we determined it independently from the 3-D basin structure. Kamae & Irikura [1998] showed that they can simulate the observed data at KBU using a relatively simple source model by a semi-empirical Green's function method. The model consists of three asperities, one on the Awaji side and two on the Kobe side. When we use this model, synthetics at KBU shows remarkable fit to the observed data but the synthetics at JMA and Motoyama First Elementary School by CEORKA (MOT) are not reproduced so well. We start from this source model and modify it by a forward modeling procedure to simulate deconvolved bedrock motion at JMA [Kawase, 1996] and the time differences of pulses at KBU and MOT. Since we are only concerned with the sites in Kobe here, we only model asperities on the Kobe side. This will not affect the final response so much because the fault on the Awaji side ruptures toward southwest, i.e. the direction of backward directivity for Kobe, so that it would not produce significant amplitude toward the Kobe side.

We assume that in each asperity rupture starts from the lower southwest corner and propagates radially, in the same manner as Kamae & Irikura [1998] assumed. The rupture speed is set to be 2.8 km/s. We only consider pure strike-slip mechanism. With these assumptions we determine a four-asperity model that simulates the deconvolved bedrock motion at JMA and explains time differences of pulses at KBU and MOT. We only consider the N33°W component when we evaluate the source model. Fig. 4 shows the source model that we would like to propose. All the asperities are on planes with the same strike of N53°E extending from the epicenter (34.603°N, 135.028°E) at the depth of 21.6 km. The first three asperities counting from west have a dip of 90° but the fourth one has 85°. The seismic moment, size, starting time of rupture, slip duration, total slip, and slip velocity function for each asperity are listed in Table 3. Fig. 5 shows the synthetics at JMA using a flat layered velocity model of rock calculated by the wavenumber integration method [Hisada 1995], together with the deconvolved bedrock motion. We can see that the synthetic waveform fits the observed data quite well.

3-D BASIN RESPONSE

Among 14 observation sites shown by solid squares in Fig. 2 we have only two stations which are considered to be on a outcrop of the rock formation, namely KBU and SKB (on the basement of a high-rise building near the JR Shin-Kobe station observed by Takenaka Corp.). All the other sites, from left to right in Fig. 2, TKT (Takatori station by JR), NTT (NTT Kobe by NTT), JMA, PIS (Port Island borehole by Kobe City), KKJ (Kobe Harbor Office by PHRI), FKA (Fukiai Gas station by Osaka Gas), KD8 (Kobe 8th pier by PHRI), RKI (Rokko Island by Sekisui House), SKH (Shin-Kobe electric power station by Kansai Electric Co.), MOT, HKO (Higashi-Kobe Bridge by PWRI), TKZ (Takarazuka station by JR) are on sedimentary basin or reclaimed land. Note that SKH lies on the rock side in Fig. 2 but actually it rests on the reclaimed land part in the mountain area. We use the estimated outcrop waveforms calculated from the borehole data at PIS and HKO for comparison.

The calculated velocity waveforms for the 3-D basin structure by the four asperity source model are shown in Fig. 6 for N33°W component. The solid lines are the observed data and the dotted lines are the synthetics. Seismograms are band pass filtered from 0.33 to 2.5 Hz. JMA is the site used to determine the source process and the waveform agrees well with the observed data as expected. The maximum amplitude of the synthetic waveform is a little smaller than that of the observed data but it should get closer if we take into account the surface structure around JMA. The first two pulses at most of the sites fit the observed data very well in amplitude and timing, except for KKJ where the effect of nonlinearity caused by liquefaction is so strong that the second pulse shape is distorted and arrives later than expected. Also the third pulse is strongly weakened by the phenomena. The third pulse at other sites fit fairly well, but at HKO and RKI the third positive peak arrive a little earlier than the observed. The synthetics at PIS, MOT, and NTT are well fit to the observed. The second negative peak at KBU and SKH appear to be smaller in the synthetics. Since these sites are right above the surface projection of the fault, slight change of the dip angle of the fourth asperity could change the results drastically. At SKB the synthetic has the amplitude twice as much as the observed. The site is located very close to the edge of the basin, but the seismometer was at the basement (the third floor beneath the ground) of a 38-story building, and so the influence of the soil-structure interaction should be taken into account. Note that because the polarity of the recording system in this building is considered to be opposite with respect to the other systems, all the components are reversed here. The third pulse at TKT and TKZ, which are located far off east and west from the central part of Kobe, is not well estimated. These results tell us that we may need a shallow asperity near TKT and TKZ, as Wald's inverted source process suggests [Wald 1996]. We need further data constraint to delineate the rupture process in the shallow part of the fault.

The peak ground velocity (PGV) distribution based on our 3-D calculation is shown in Fig. 7 (again N33°W component). Since the original drawing is in color, it is a little difficult to see the high amplitude regions. Basically white regions correspond to the areas of about 70 to 90 cm/s in PGV and darker areas inside the white regions correspond to the high amplitude regions whose PGVs are in the range of 100 to 130 cm/s. It is apparent that our simulation succeed to reproduce the disaster belt quite nicely extending from east to west in the main part of the Kobe area and the south-western part of Nishinomia City. We should note that this high amplitude belt is not uniform in its PGV values. As is the distribution of the damage ratios we observe here lateral fluctuations inside the high amplitude belt. To understand the cause of the high amplitude region we then calculate the basin response without the edge-induced waves. It is accomplished by introducing an energy absorbing layer only on the surface of the Rokko Granite. In this model the S-wave arrivals in the rock-side are totally suppressed and so we can see the real amplitude of the direct S-waves in the basin-side. Fig. 8 shows the PGV distribution of the model without S-waves in the rock-side (a large black region in the rock side represents the amplitude suppressed area). It is clear that the basin-side S-waves themselves are small in amplitude and

homogeneous in their distribution and therefore we cannot see any strong lateral variation as seen in Fig. 7. It is clear now that we need the edge-induced diffracted/surface waves, in another word, “the edge effect” in order to have a clear belt-like shape of the high amplitude region.

CONCLUSIONS

Using a 3-D basin structure and a relatively simple four asperity source model, we evaluate strong motions at the observation sites. The results show that with this combination it is possible to simulate strong ground motion for a wide area quite accurately. For sites on the reclaimed land we need to include nonlinear amplification effect of the shallow surface layers to further improve the fit. For sites near the ends of the fault we cannot reproduce the observed record without introducing shallow asperities. In conclusion we make it clear that we need detailed information of the source and the site to simulate near-field strong motions quantitatively. Thus we must establish the methodology on how to predict such information for future disastrous earthquakes.

ACKNOWLEDGEMENT

The observed records used for comparison were collected by each observation organisations and distributed directly or through Architectural Institute of Japan (for JR data, serial no. R31). We would like to appreciate the hard work they must have gone through to collect and distribute these data. We also benefited from the Simultaneous Simulation experiment conducted by the Japanese Working Group on ESG as a special effort in ESG98. We thank Dr. Y. Hisada for the use of his wavenumber integration code.

REFERENCES

- Endo, S., S. Watanabe, M. Makino, A. Urabe, H. Aso, Y. Koreishi, and S. Ejiri [1996]. “Elastic wave reflection survey in Ashiyagwa line”, *Monthly Report of Geological Survey of Japan*, 47, pp79-94 (in Japanese).
- Graves, R.W. [1996]. “Simulating seismic wave propagation in 3D elastic media using staggered-grid finite differences”, *Bull. Seismo. Soc. Am.*, 86, pp1091-1106.
- Hisada, Y. [1995]. “An Efficient Method for Computing Green's Function for a layered Half-Space with Source and Receivers at Close Depth (Part 2)”, *Bull. Seismo. Soc. Am.*, 85, pp1080-1093.
- Kagawa, T., S. Sawada, Y. Iwasaki, and S. Emi [1990]. “Osaka basin structure from explosion survey”, *Zisin*, Ser. 2, Vol. 43, pp527-537 (in Japanese with English abstract).
- Kamae, K. and K. Irikura [1998]. “Source model of the 1995 Hyogoken Nanbu earthquake and simulation of near-source ground motion”, *Bull. Seism. Soc. Am.*, 88, pp400-412.
- Kawase, H., T. Satoh, T. Fukutake, and K. Irikura [1995]. “Borehole records at Port Island in Kobe observed during the Hyogo-ken Nanbu earthquake and its simulation”, *Trans. of Architectural Institute of Japan*, No.475, pp83-92 (in Japanese with English abstract).
- Kawase, H. [1996]. “The cause of the damage belt in Kobe: The Basin-edge effect, Constructive interference of the direct S-wave with the basin-induced diffracted/Rayleigh waves”, *Seismo. Res. Lett.*, 67, No.5, pp25-34.
- Kawase, H., S. Matsushima, R.W. Graves, and P.G. Somerville [1998]. “Three-dimensional wave propagation analysis of simple two-dimensional basin structures with special reference to “the basin-edge effect”, -The cause of the damage belt during the Hyogo-ken Nanbu earthquake-”, *Zisin*, Ser. 2, pp431-449 (in Japanese with English abstract).
- Kobayashi, Y., Y. Kinugasa, A. Hasegawa, T. Ikawa, M. Ohnishi, and S. Mizohata [1996]. “Reflection survey in Higashinada-ku, Kobe-shi”, *Abstract, Seismo. Soc. Japan*, No.2, A38 (in Japanese).
- Satoh, T., T. Sato, and H. Kawase [1993]. “S-wave velocity and nonlinearity identification of a sedimentary basin, -Weak and strong motion analysis observed in borehole in Kuno, Ashigara”, *Trans. of Architectural Institute of Japan*, No.449, pp55-68 (in Japanese with English abstract).
- Sekiguchi, H., K. Irikura, T. Iwata, Y. Takehi, and M. Hoshiba [1996]. “Minute locating of faulting beneath Kobe and the waveform inversion of the source process during the 1995 Hyogo-ken Nanbu, Japan, earthquake using strong ground motion records”, *J. Phys. Earth*, 44, pp473-487.
- Wald, D.J. [1996]. “Slip history of the 1995 Kobe, Japan, earthquake determined from strong motion, teleseismic, and geodetic data”, *J. Phys. Earth*, 44, pp489-503.

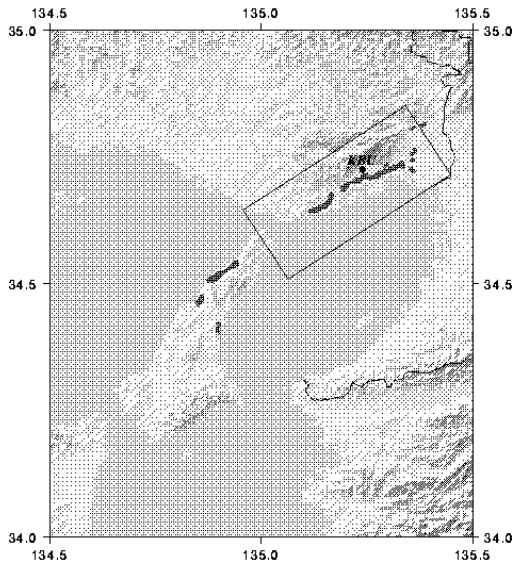


Fig.1 Map of the Osaka basin and the area of the 3-D FDM simulation.

Table 1 Velocity model inside the basin

Layer	Vp (km/s)	Vs (km/s)	ρ (g/cm ³)	Q	Thickness ratio
1	1.70	0.40	1.75	20	0.08
2	1.85	0.50	1.85	25	0.12
3	2.20	0.70	2.10	35	0.25
4	2.50	1.10	2.30	55	0.55

Table 2 Velocity model of rock and crust

Layer	Vp (km/s)	Vs (km/s)	ρ (g/cm ³)	Q	depth (km)
1	2.50	1.00	2.00	50	0.00
2	3.20	1.80	2.10	100	0.08
3	5.15	2.85	2.50	200	0.40
4	5.50	3.20	2.60	400	0.56
5	6.00	3.46	2.70	600	5.04
6	6.70	3.87	2.80	700	18.0
7	7.50	4.33	3.00	800	34.5

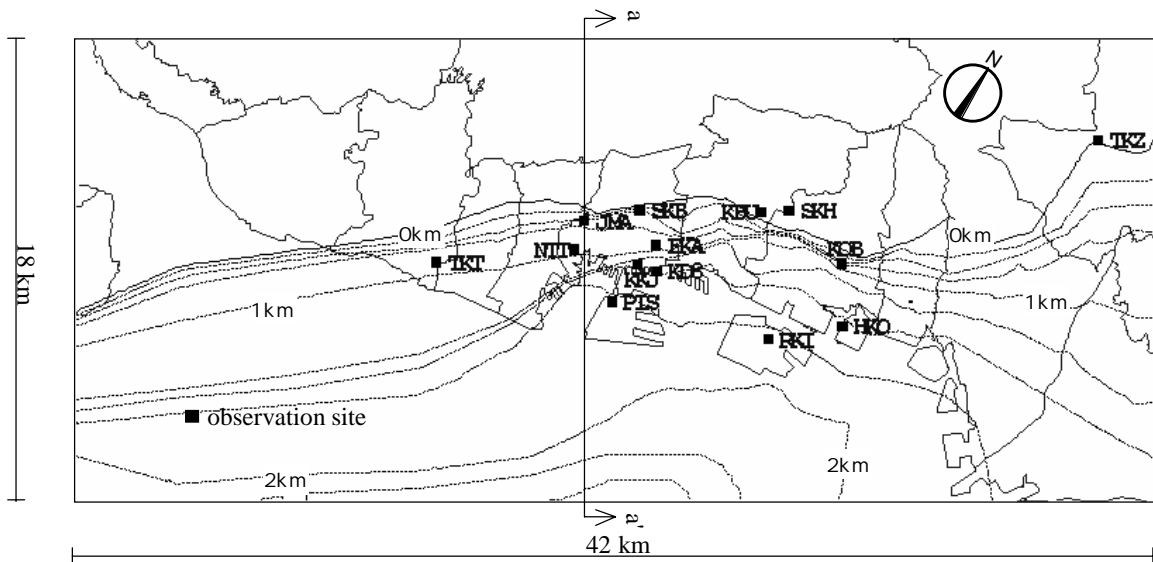


Fig.2 Contour map of the bedrock depth of the 3-D basin structure model with the mainshock observation sites. Line a-a' shows the section line of Fig.3.

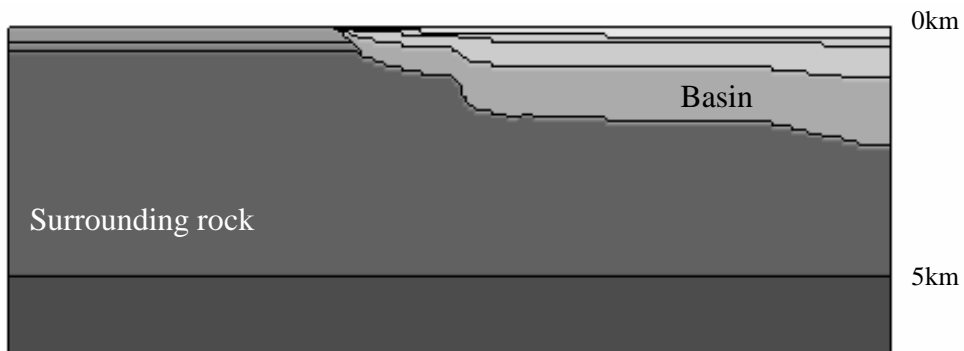


Fig.3 Cross section of the 3-D basin structure at line a-a' in Fig.2.

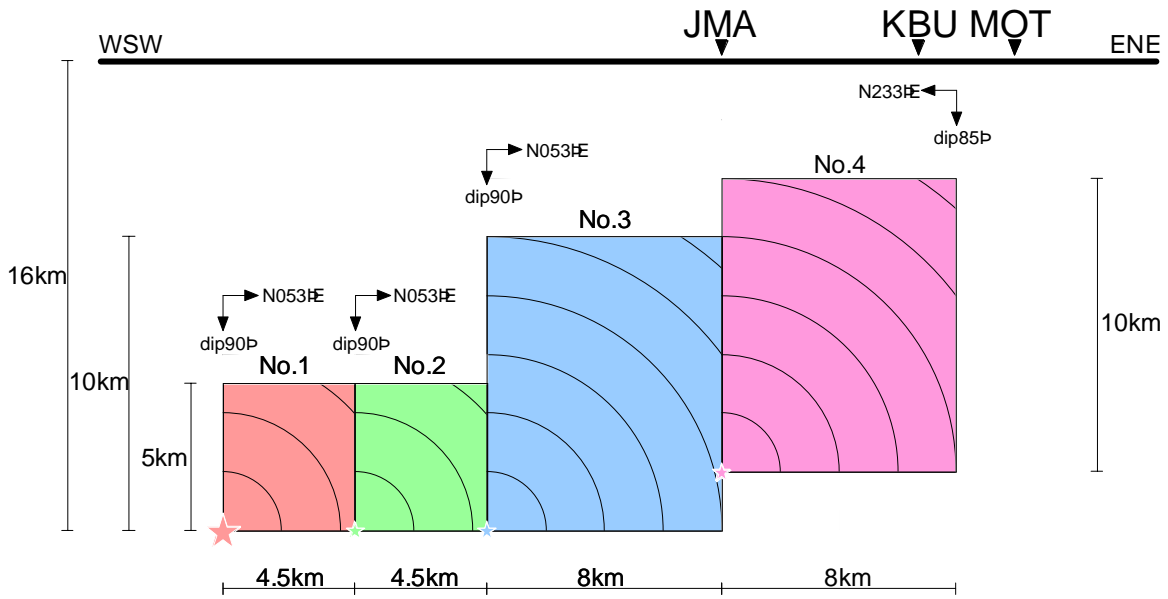


Fig.4 Four asperity model derived from the forward modeling in this study. Hypocenter is shown by a large star while a rupture initiation point is shown by a small star for each asperity.

Table 3 Fault parameters for each asperity

No.	M_0 $\times 10^{18}$ [Nm]	size LxW [km ²]	start of rupture [sec]	total slip [m]	slip velocity function
1	0.62	4.5 x 5	0.00	0.85	400kine 0.42s
2	1.07	4.5 x 5	1.79	1.47	815kine 0.66s
3	2.59	8 x 10	3.70	1.00	210kine 1.20s
4	4.83	8 x 10	6.25	1.90	330kine 1.50s
total	9.11	205			

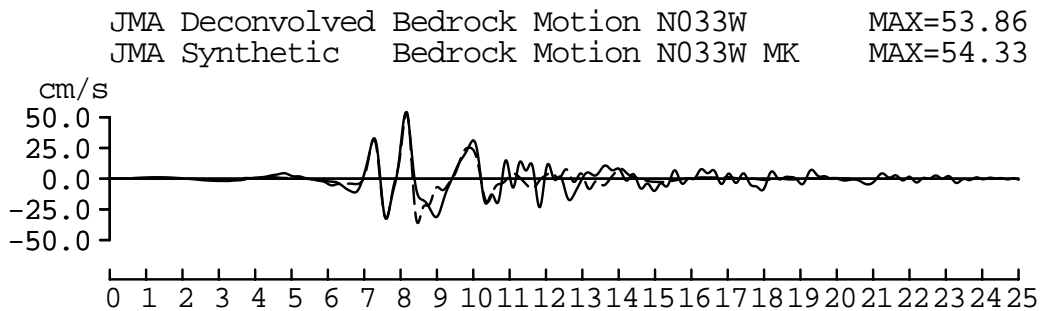


Fig. 5 Comparison of synthetic velocity seismogram at JMA with deconvolved bedrock motion (i.e., observed). The synthetic seismogram is shown by a dotted line while the observed by a solid line.

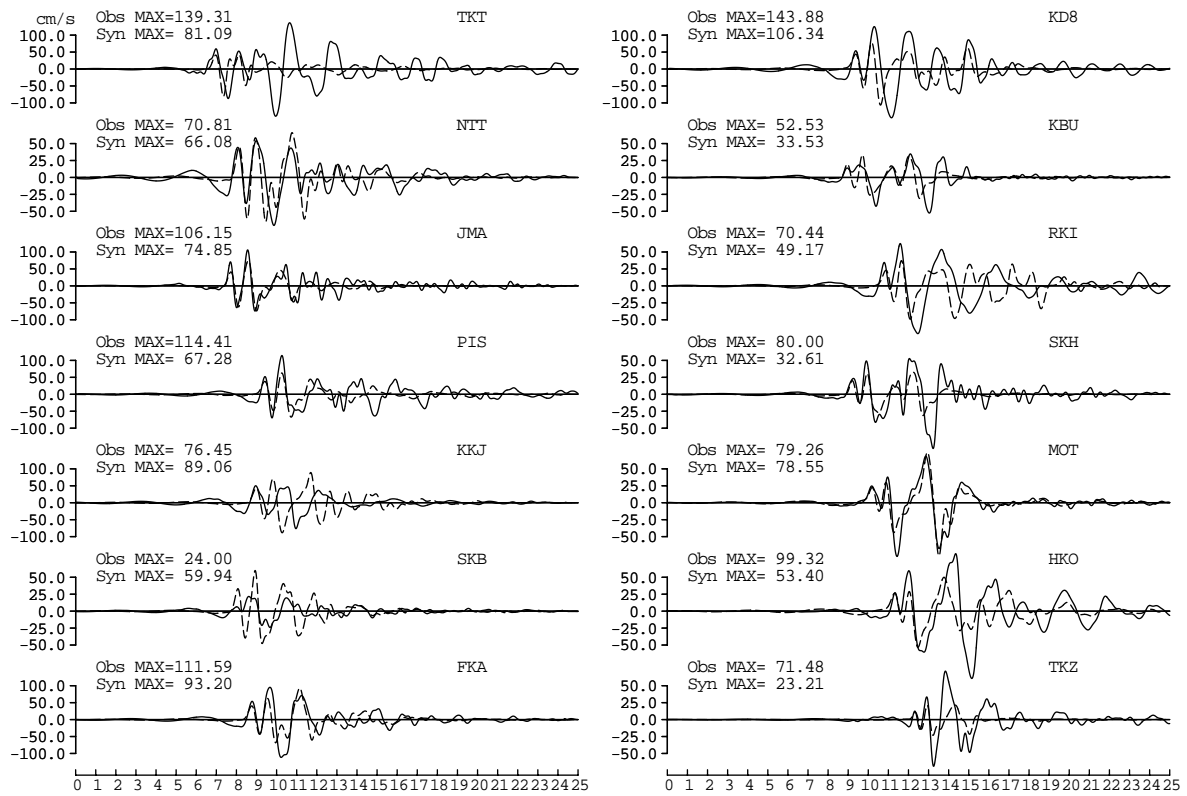
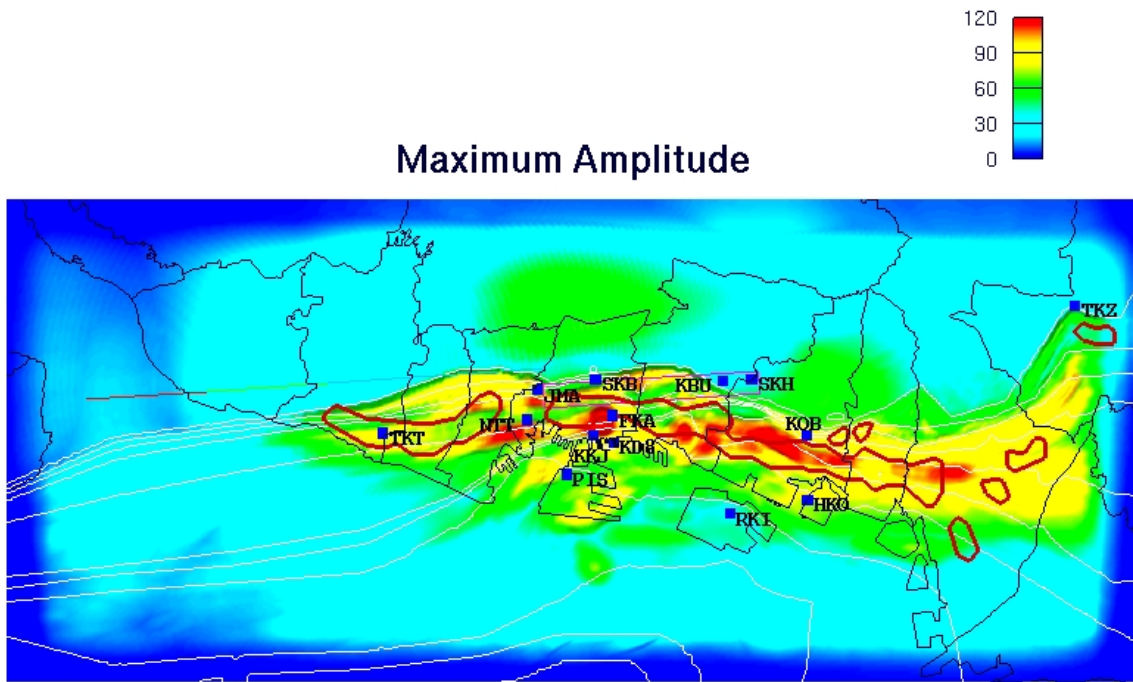
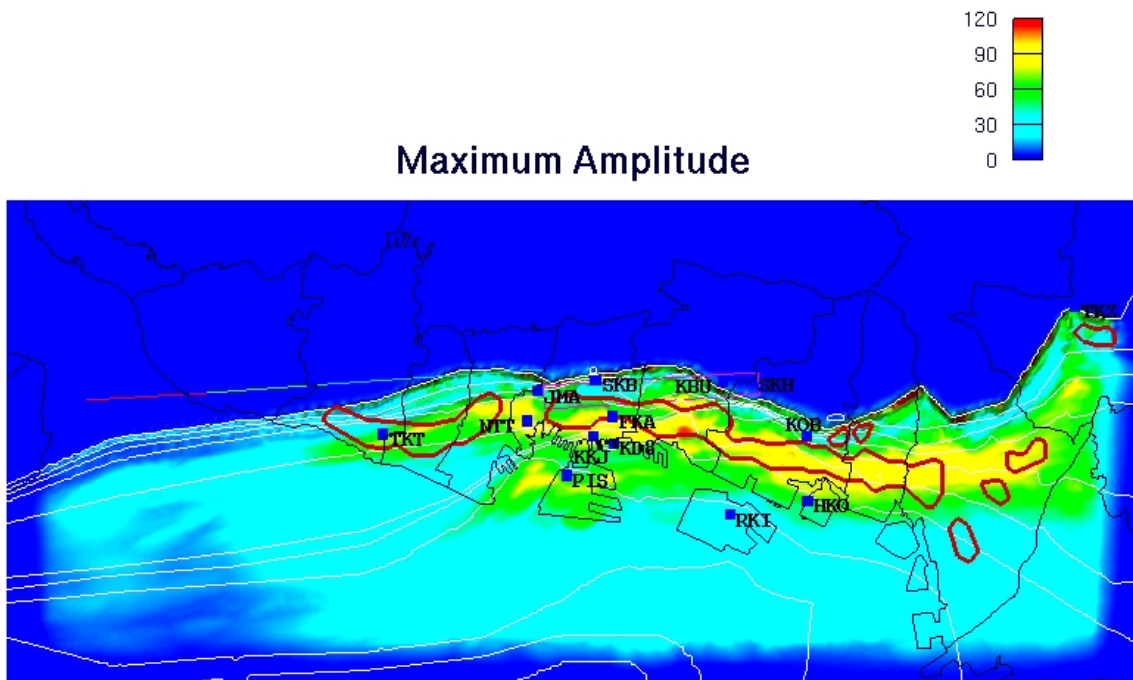


Fig.6 Comparison of synthetic velocity seismograms with the observed records for 14 sites in the modeled region. The synthetic seismograms are shown by dotted lines while the observed ones by solid lines.



**Mainshock of the Hyogo-ken Nanbu Earthquake of 1995
short 4th asperity model**

Fig.7 Peak ground velocity distribution calculated by the 3-D basin and 4-asperity model



**Mainshock of the Hyogo-ken Nanbu Earthquake of 1995
short 4th asperity model
rockScut**

Fig.8 Peak ground velocity distribution calculated by the rock-side S-wave cut model to suppress the edge effects. The whole black region in the upper half is the S-wave suppressed rock-side.